DESIGNING AND MODELLING OF CONTACTLESS ELECTRIC-VEHICLES BATTERY- CHARGING STATION FED FROM PHOTO-VOLTAIC ARRAY

Essamudin A. EBRAHIM
Power Electronics and Energy Conversion Department,
Electronics Research Institute (ERI)
El-tahrir Street, 12622 Dokki, Cairo, Egypt
essamudin@yahoo.com, essamudin@eri.sci.eg

***Abstract*:** *The development and commercialization of hybrid electric vehicles (HEVs) and electric vehicles (EVs) are actively being realized due to environmental concerns and rising oil prices. But, EV technology with battery has faced many problems up to now. One of the most important problems is rapidly battery-charging from a clean and reliable source. So, this research proposes a convenient way to charge batteries of EVs and HEVs from a neat power supply. The paper introduces a public off-board battery-charging station fed from on-grid (OG) photovoltaic (PV) array. The proposed 100Kw-contactless charging station is modeled, designed and simulated. It comprises two main sections: station-side (stationary) section and EV (moving) section. The first section includes PV panels, maximum power point tracking (MPPT)-converter, on-grid 3-level interface inverter, and high-frequency compensated resonant converter. The second one consists of the rectifier, switched mode power converter, and battery-charging controller. An inductive-coupled power (ICP) is transferred from the station to the batteries through an air-core transformer (ACT) with large air-gap. Its primary winding is placed on the station ground and the secondary winding is in the EV. Modeling of the ACTs accomplishes several requirements such as air-gap, have good tolerance to misalignment, light-weight, durable and cost effective as possible. Smart and intelligent controllers are proposed for MPPT, interface on-grid inverter and battery-charging converter. Simulation results are obtained using a Simulink/m-file software package helping in modeling of battery-charging public station.*

Keywords: *Contactless Battery Charger, Inductively-Coupled Power Transfer (ICPT), Air-Core Transformer (ACT), Photo-Voltaic (PV),*

1. Introduction

Several efforts have been exerted to develop vehicles utilizing environmentally friendly power source to replace the conventional internal combustion engine (ICE). Electric Vehicles (EVs) and Fuel Cell Electric Vehicles (FCEVs) have been typically proposed to replace these conventional vehicles in the near future.

As generally recognized, electric vehicles can achieve higher energy conversion efficiency, motor-regenerative braking capability, fewer local exhaust emissions, and less acoustic noise and vibration, as compared to ICEs. The traction battery has an important role in the development of EVs and hybrid electric vehicles (HEVs). Charging process of these batteries needs to be quick, safe, easy, and low cost. Mostly, charging process is achieved by using outdoor plug-in power supply through a large cable. Contact-based charging system creates a major inconvenience and a safety hazard for car owners. Inductive-coupled power transfer (ICPT) contactless-charging system introduces an imperative solution for the safety hazard and inconvenience problems, through transferring the charging energy over a weakly magnetic coupler [1-3].

Through the last decade, several aspects of ICPT have been studied, such as magnetic coupler design techniques, compensation topologies, control methods, foreign object detection algorithms, and the radiation safety issues [4-6]. Also, one of the most important considerations for the ICPT charging station is the main power supply that should be environmental friendly. High quality photo voltaic (PV) cells – as a renewable energy source- are nowadays available with acceptable price [7]. Some few researches – as in [8] - proposed a 100-KW public station fed from PV source - with storage elements - for partial charging (30%) only and (10%) of the required power is supplied from the PV-array. This system uses very bulky and expensive batter bank storage as a storage element in the public

charging station. Also, in [15], the author presented a charge controller of solar photo-voltaic panel (SPV) fed battery. But in [16], authors proposed a design of a docking station for solar charged electric and fuel cell vehicle. The purpose of this study is to provide an alternative to manufactures and consumers to encourage the use of clean energy systems for transportation purposes. As seen above, most of these researches introduce a simulation or practical study with limited or certain applications.

So, this paper introduces a software package for modelling, designing and simulation of a battery - charging station fed from on-grid PV array. Two main power supplies are proposed: the main grid and PV array without any storage elements. This package includes the modelling of the PV array with its MPPT algorithm, its boost converter with proposed smart control and three-level inverter required to interconnect between the main grid and the PV array. In addition, a high-frequency resonant converter with series compensation is modelled and simulated through this study. Also, a Matlab/ m-file software package is included to design air-cored transformer (ACT) required for contactless inductively coupled power transfer (ICPT). The system also uses a Buck converter as a battery-charging controller with bacteria foraging optimization PI (BFO-PI) tuning. The package is used to charge four Lithium- Ion batteries of Honda EV in order to test the capacity and efficiency of the station.

2. The proposed ICPT-PV for EV public-charging station

The proposed 100-Kw ICPT-PV public-charging station comprises two main parts (as shown in figure 1) : the station side and EV section. The capacity of the station depends on its rated power and the several EV batteries types. The average rated power for most types of the battery vehicles is approximately (20 KWh). The EV side includes secondary winding of ACT with its resonant series compensation, uncontrolled bridge rectifier with smoothing capacitor, buck converter – as switched mode - to control dc-voltage charging level with its smart control, and EV-batteries.

3. The primary (station) side

The primary-side consists of PV-array as a neat-renewable energy source with its maximum power point tracking (MPPT) control algorithm including boost converter, main-grid with a bi-directional 3-level inverter for interfacing with PV-array, high-frequency resonant converter with series compensation and the primary winding of the air-core transformer (ACT).

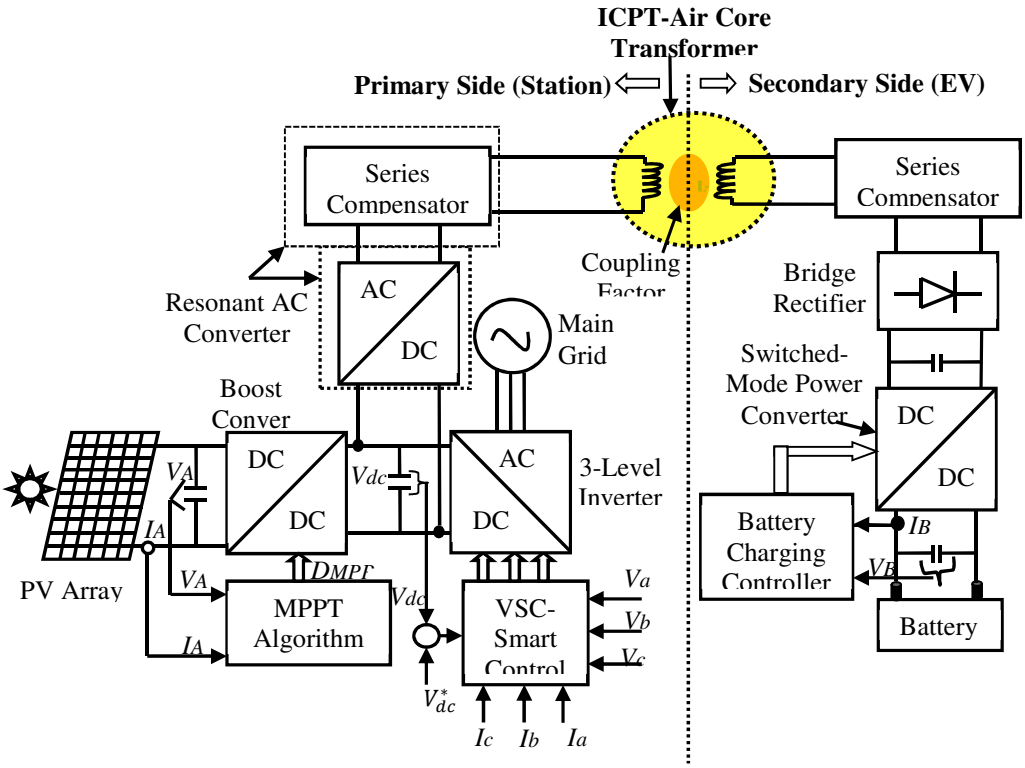

Figure 1. The proposed ICPT system for battery charging fed from PV-array

3.1. Modelling of the PV array with MPPT algorithm

The mathematical models of PV cell, module and array are obtained from [7] as follow:

The total cell current can be computed as:

$$I = I_{irr} - I_o\left[e^{\left(\frac{q(V+IR_S)}{nkT}\right)} - 1\right] - \frac{V+IR_S}{R_p} \quad (1)$$

The total module current can also computed as:

$$I_M = I_{irr} - I_o\left[e^{\left(\frac{q(V_M+I_M N_S R_S)}{N_S nkT}\right)} - 1\right] - \frac{V_M+I_M N_S R_S}{N_S R_p} \quad (2)$$

Dependently, the total current of PV array is:

$$I_A = N_p I_{irr} - I_o\left[e^{\left(\frac{q\left(V_A+I_A\frac{N_S}{N_p}R_S\right)}{N_S nkT}\right)} - 1\right] - \frac{V_A+I_A(\frac{N_S}{N_p})R_S}{\frac{N_S}{N_p}R_p} \quad (3)$$

Where,

I, I_M, I_A *cell, module, array currents (A)*
I_{irr} *irradiance or photo current (A)*
I_o *The diode saturation current (A)*
V, V_M, V_A *The cell, module and array voltages (V)*
$q = 1.6 \times 10^{-19}\ C$
$K = Boltzmann\ constant = 1.3806503 \times 10^{-23} J/K$
R_s, R_p *series and parallel resistance (Ω)*
$N_s N_p$ *number of series and parallel cells*
T *the temperature of the cell (°K)*

The proposed station is fully energized from on-grid 100-Kw PV array through the day only without any storage elements and through the night it will be supplied from the main grid. So, the number of series and parallel modules can be computed as follow:

The total power required = 100 Kw, the total output PV-array voltage = 300 V, if the SunPower modules (SPR-305) type [9,10] is used with its characteristics: open-circuit voltage: V_{oc}= 64.2 V, short-circuit current: I_{oc} = 5.96 A, voltage and current at maximum power: V_{MPP} =54.7 V, I_{MPP}= 5.58 A, $\therefore N_s = \left(\frac{300}{64.2}\right) = 4.6 \cong 5$ modules, then, the dc output terminal voltage of the PV array will be 320V. Each module produces maximum power = $(54.7 \times 5.58) \cong 305\ W$, dependently, the total required number of modules can be obtained as: $\left(\frac{100000}{305}\right) = 327$ modules= $N_s \times N_p$, then, the total parallel modules can be given as: $(327/5) \cong 66$ modules, then, the total number of modules are $(66 \times 5 = 330)$ and dependently, the maximum power can be recomputed as:P_{MPP}=(330×305)/1000=100.65 Kw,

If the dimension of one module is $(1.559m \times 1.046m = 1.63m^2$[11]), then, the total surface area required on the station roof should be $(1.63 \times 330 \cong 538\ m^2)$, the modules can be arranged in rows and columns above the roof of the station. However, the V-I and V-P characteristics of both one module and the PV-array are shown in figures 2 (a and b) respectively.

3.2. Maximum power point tracking (MPPT) algorithm with boost converter

There are several methods are proposed to achieve MPPT [12,17]. One of the most popular and simple method is the incremental conductance (IC) method. This method is based on the fact that the power slope of the PV is zero at MPP (dP/dV = 0), positive in the left and negative in the right, as shown in ig. 2(a,b). Due to this condition, the MPP can be found in terms of the increment in the array conductance. Using (4) it is possible to find the IC conditions presented by (5).

$$\frac{dP_A}{dV_A} = \frac{d(V_A.I_A)}{dV_A} = I_A + V_A\frac{dI_A}{dV_A} = \text{error} \quad (4)$$

$$\frac{\Delta I_A}{\Delta V_A} = -\frac{I_A}{V_A}\ (5a) \text{ or } \frac{\Delta I_A}{\Delta V_A} > -\frac{I_A}{V_A}\ (5b) \text{ or } \frac{\Delta I_A}{\Delta V_A} < -\frac{I_A}{V_A}\ (5c)$$

Where (5a) represents the condition at MPP, (5b) represents the condition in the left and (5c) in the right of MPP. This method searches the MPP in the same way as P&O, and also features a modified version, but it is not necessary to calculate the PV output power and presents very good transient performances when subjected to rapidly changes in atmospheric conditions.

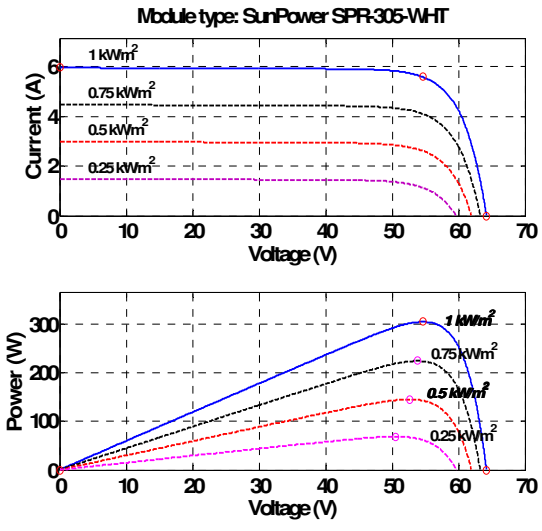

(a) One module

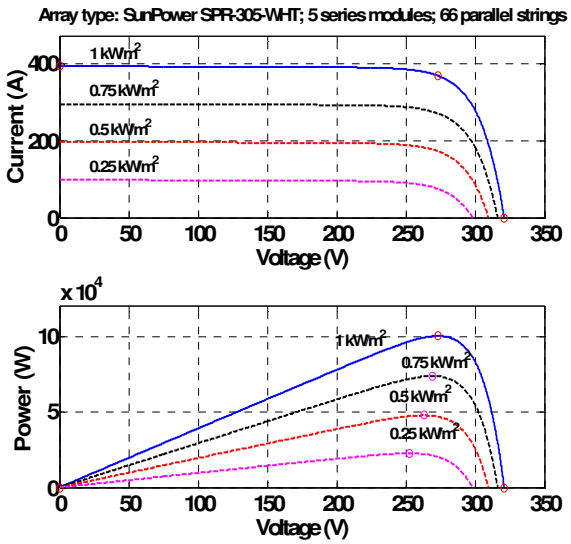

(b) PV array

Figure 2. V-I and V-P characteristics for (a) one module and (b) for the PV array

To minimize the error signal (e), integral regulator is used and the duty cycle at MPP can be given as:

$$D_{MPP} = K_I \int_0^{\Delta t} \left(\frac{\Delta I_A}{\Delta V_A} + \frac{I_A}{V_A}\right) dt \qquad (6)$$

Finally, the output duty cycle is obtained as analogue signal that can be easily added with a saw-tooth triangular waveform with high frequency to produce a high frequency triggering square-wave pulses required to turn on and off the IGBT- boost converter switch. The Matlab/Simulink of this algorithm is illustrated in figure (3).

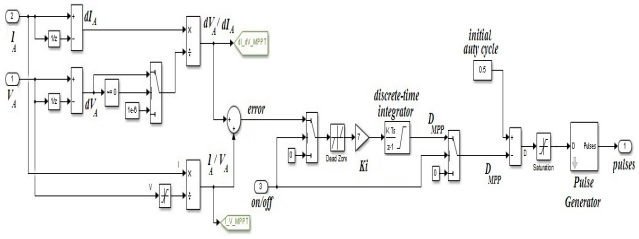

Figure 3. Matlab/ Simulink MPPT algorithm with boost-converter pulse generation

3.3. Boost converter

The boost converter is used to boost PV output voltage from 320V to 540. It comprises series inductor with shunt capacitor both are controlled by using IGBT as an electronic switch that is derived from MPPT-algorithm output through the duty-cycle changing. The boost converter is shown in figure 4.

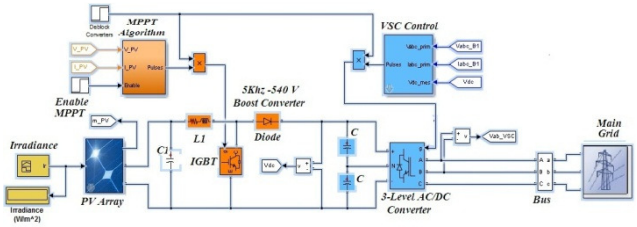

Figure 4. Modelling of on-grid PV-array with MPPT-converter and inverter set

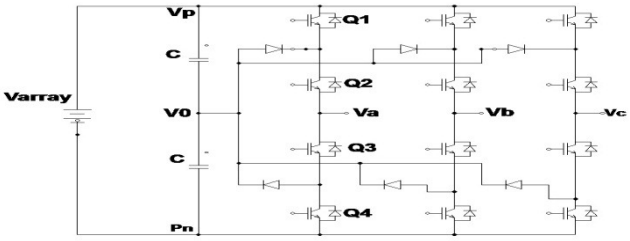

Figure 5. Three-phase 3-level inverter (power circuit)

3.4. Three-phase 3-level voltage-controlled (AC/DC converter) inverter

To interconnect between the dc- output of the PV and the main ac-grid, it should be use a bi-directional converter to transfer power from dc-side to ac-one and vice versa. So, a 3-level voltages-source current - controlled converter with neutral point clamped (NPC) is proposed. Figure 5 shows the circuit configuration of the NPC inverter. Each leg has four IGBTs connected in series. The applied voltage on the IGBT is one-half that of the conventional two-level inverter. The bus voltage is split in two by the connection of equal series connected bus capacitors. Each leg is completed by the addition of two clamp diodes. The main advantages of this technique are its capability of handling higher voltages, lower line-to-line and common-mode voltage steps and lower output current ripple for the same switching frequency as that used in a two level inverter.

This converter can produce three voltage levels on the output: the DC bus plus voltage (V_p), zero voltage (V_0) and DC bus negative voltage. For a one phase (phase a) operation, when IGBTs Q_1 and Q_2 are turned on, the output is connected to V_p; when Q_2 and Q_3 are on, the output is connected to V_0; and when Q_3 and Q_4 are on, the output is connected to V_n[13].

3.5. Voltage-source DC/AC converter/inverter control

The output of the boost converter is variable and should be maintain constant at a certain level (equal

or greater than the maximum power ac supply of the main grid), so, the actual and reference dc-link voltage is controlled by using PI controller that its parameters (K_p, K_i) are tuned by using bacteria-foraging optimization algorithm (BFO), where, $(e_v = V_{dc}^* - V_{dc})$. This controller is known as PI-BFO and the complete algorithm is explained in [7]. The ac-grid line to line voltage equal 380V, so, the dc-link voltage maintains at ($380\sqrt{2}$ ≅540V). Also, the power factor of the inverter is maintained constant at unity. This can be achieved by making $I_{qs}^* = 0$. In addition, another intelligent PI-BFO controller is used as a current regulator for direct reference and actual current components $(e_i = I_{ds}^* - I_{ds})$. The overall control algorithm and the Matlab/Simulink blocks are shown in figure 6. The output voltage frequency is equal to 50 Hz and PWM frequency is 30 KHz.

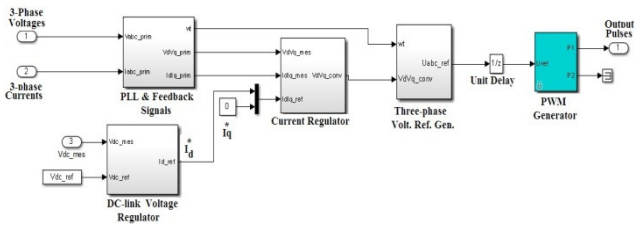

Figure 6 Control algorithms for dc-link voltage and current regulator for 3-level inverter

3.6. Modelling of contactless power-transfer air-core transformer (ACT)

An ICPT system should efficiently delivering power from a stationary primary source to a movable secondary source over a relatively large air gap. In this system, power is magnetically transferred from the primary winding to the secondary winding of specially constructed transformer. Some of these proposed transformer configurations have a magnetic core and others have an air core. Factors that influence the choice of transformer are air gap between the primary and secondary winding, cost of the magnetic material core, weight of the core, eddy current losses in the core, operating frequency and sensitivity to misalignment between primary and secondary windings.

The air gap in the transformer configuration is large; so, this configuration has a large leakage inductance and low mutual coupling which implies large magnetizing current. Since CPT transformer with air core is light in weight and has no core losses, so, in this study, CPT transformer with air core is considered. The power transfer capability of an ICPT system depends directly on the coupling coefficient, k which is given by: $k = \frac{M}{\sqrt{L_1 L_2}}$, where L_1 and L_1 are the self-inductance coefficients of the primary and secondary coils and M is the mutual inductance between them. The schematic diagram of the transformer is shown in figure (7-a) and the equivalent circuit of the model is illustrated in (7-b), where $L_p and\ L_s$ are the leakage inductance of both primary and secondary windings of the ACT.

To improve the power transfer capability to the load, it is necessary to include capacitors in both sides. By working at the resonance frequency in the secondary selecting the appropriate capacitor C_2, the power transferred to the load has a maximum value. Selecting the capacitor in the primary side C_1at this frequency, the total impedance of the system is purely resistive, so the current is in phase with the voltage and the source needs to deliver the minimum apparent power.

If Series–Series (SS) compensation is selected (i.e. both primary and secondary capacitors are connected in series with the respective coils as shown in figure 7-c), the primary capacitance is independent of both the magnetic coupling and the load [1]. The power transferred from the primary to the secondary is given by:

$$P_2 = \frac{\omega_0^2}{R_L} M^2 I_p^2 \qquad (7)$$

Where, ω_0, I_p, R_L are the resonant frequency, primary current and the load resistance respectively. The value of ω_0 is chosen equal for both primary and secondary winding and can be computed as:

$$\omega_0 = \frac{1}{\sqrt{L_p C_1}} = \frac{1}{\sqrt{L_s C_2}} \qquad (8)$$

So, the capacitance values for both primary and secondary windings C_1 and C_2 can be obtained from:

$$C_1 = \frac{1}{L_p \omega_0^2} \quad \text{and} \quad C_2 = \frac{1}{L_s \omega_0^2} \qquad (9)$$

Designing of ACT depends on the values of its parameters $L_1, L_2\ and\ M$ that can be calculated from geometrical dimensions. Rectangular coils for both primary and secondary are selected for the proposed ACT because of giving much better tolerance to misalignment (as shown in figure 8). The design process is achieved according to the flow chart illustrated in [3] and the overall ACT parameters for 100KW charging station are tabulated in table 1.

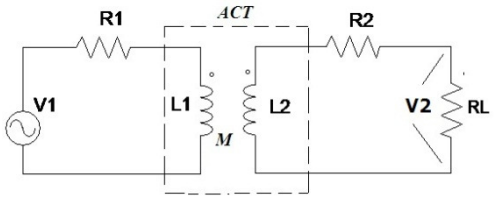

(a) Schematic diagram

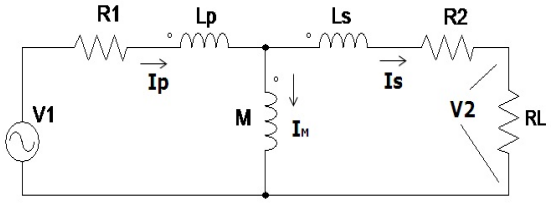

(b) Equivalent circuit

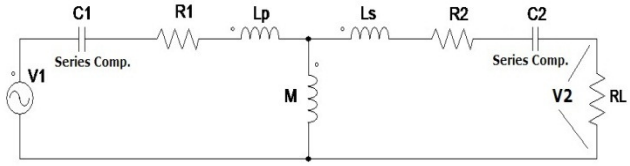

(c)Equivalent circuit with SS-compensation

Figure 7 Modelling of an ICPT air-core transformer with SS-compensation

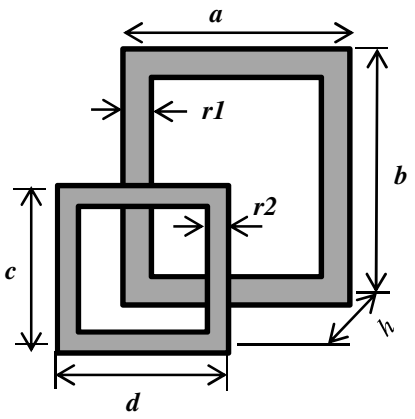

Figure 8 geometrical dimensions of the proposed ACT

The Matlab m-file is used to simulate the ACT and a software package is designed and it is accurate for any ACT with a rectangular form. The parameters of rectangular coils for any dimension and any relative position between them are presented.

3.7. Resonant DC/AC high frequency converter

DC-link output voltage cannot be transferred directly to the AC-transformer. So, a resonant ac converter is required. This converter is a single-phase bridge inverter switched at a very high resonant frequency as shown in figure 9. The output of the converter is fed to the primary winding of the air-core transformer through a series compensated capacitor.

4. Secondary Side (EV Side)

The secondary-winding of the ACT is mounted on the EV side with inductive coupling with primary winding through air-gap. This side (as shown in figures 1 and 10) includes single-phase uncontrolled bridge rectifier, switched-mode power buck converter with its intelligent battery-charging controller, and tracking batteries.

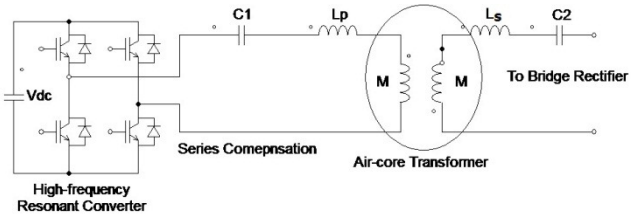

Figure 9. The high-frequency resonant converter with SS-compensation of ACT

4.1. DC/DC Buck converter

This converter is used to reduce the input voltage to the suitable value required to charge batteries. As shown in figure 10, it consists of an IGBT as a controlled switch, diode, series reactor and shunt capacitor. A feed-back signal of the battery-charging terminal voltage is compared with a reference required value and the error signal is controlled by using PI-BFO smart controller. The control diagram is shown in figure 11.

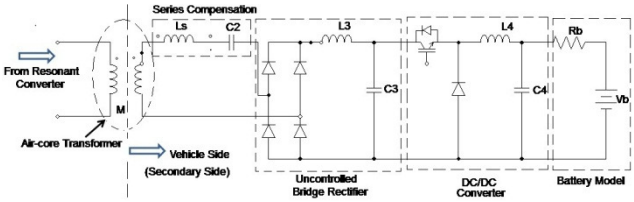

Figure 10. Components of the Electric Vehicle section (secondary side)

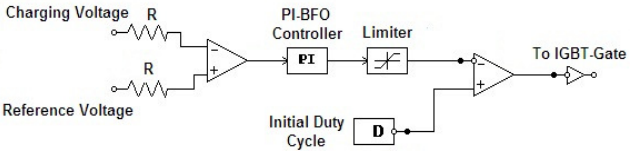

Figure 11. The contorl circuit of Buck-converter

4.2. Mathematical model of EV-battery

The actual mathematical dynamic model of EV-battery for simulation will be obtained from [14,18] as follows:

4.2.1. For Lead Acid battery:

Charging:

$$V_{bat} = E_0 - R.i - K\frac{Qi^*}{(it-0.1\,Q)} - K\frac{Qit}{(Q-it)} + e^t \quad (10)$$

Discharge: $V_{bat} = E_0 - R.i - K\frac{Q(it+i^*)}{(Q-i.t)} + e^t \quad (11)$

4.2.2. Li-Ion Battery:

Charging:

$$V_{bat} = E_0 - R.i - K\frac{Qi^*}{(it-0.1\,Q)} - K\frac{Qit}{(Q-it)} + Ae^{-B.it} \quad (12)$$

Discharge:

$$V_{bat} = E_0 - R.i - K\frac{Q(it+i^*)}{(Q-it)} + Ae^{-B.it} \quad (13)$$

4.2.3. NiMH and NiCd battery:

Charging:

$$V_{bat} = E_0 - R.i - K\frac{Qi^*}{(|it|-0.1\,Q)} - K\frac{Q.it}{(Q-it)} + e^t \quad (14)$$

Discharge: $V_{bat} = E_0 - R.i - K\frac{Q(it+i^*)}{(Q-it)} + e^t \quad (15)$

Where**,**

V_{bat}= battery voltage (V), E_0 = battery constant voltage (V), K= polarisation constant (V=Ah)) or polarisation resistance (Ω), Q= battery capacitance (Ah), $it = \int idt$ = actual battery charge (Ah), R=battery internal resistance (Ω), i = battery current (A), i^*= battery-filtered current (A), A = exponential zone amplitude (V), B = exponential zone time-constant inverse $(Ah)^{-1}$

5. Simulation Results and Discussion

The proposed software package is used to design 100-Kw EV- battery charger public station fed from PV array. The used data of the PV array are that obtained from designing process of section 3.1. The ACT transformer required for ICPT is designed for this station and its main parameters are given in table 1. Twisted Litz conductors are used for the transformer HV winding to reduce the eddy currents.

The proposed system is tested by charging 4-EV Honda identical batteries in the same time. The capacity of one battery equal 19-Kwkh and the rated charging voltage is 200V. The charging process is done when the initial state of charging (SOC) is 30%. All controlled switches used are IGBT with voltage and current rates 1500V and 200A respectively. The irradiance of PV profile is initially considered as a constant value with 1000 W/m² and then suddenly reduced to 250W/m² at time=0.5S for 0.2 S and then increased to its initial value - as shown in figure 12-a. Figure 12-b illustrates the PV- output terminal voltage without using controller. The voltage profile is changed according to the irradiance variation. But, when using the boost converter, the controller tries to change duty cycle of the converter to track the reference dc-link voltage as shown in figure 12-e.

Table 1. Parameters of ACT

Parameter	Value
No. of primary turns (N_1)	6
No. of secondary turns (N_2)	4
Radius of the primary coil (r_1)	9.27 *mm*
Radius of the secondary coil (r_2)	8.00 *mm*
The length and width of primary coil are equal *(a,b)*	0.9 *m*
The length and width of secondary coil are equal *(c,d)*	0.6 *m*
Primary internal resistance (R_1)	1.2365 *mΩ*
Secondary internal resistance (R_2)	2.2781 *mΩ*
Self-inductance of primary (L_1)	0.082 *mH*
Self-inductance of secondary (L_2)	0.041 *mH*
Mutual inductance between coils (M)	.011 *mH*
Air gap length	175 *mm*
the coupling coefficient, k	0.2
Voltage of secondary (V_2)	500 *V*
Resonant frequency (f_0)	20 *KHz*
Power of Secondary (P_2)	100 *KW*
Primary series compensation (C_1)	0.7722 *uf*
Secondary series compensation (C_2)	1.5441 *uf*

Figure 12-c describes the duty-cycle variation with time to match the required voltage. Figure 12-d shows the mean-power of the PV-array through charging process. It can be easily notices that the mean power is reduced to a minimum value when PV-irradiance is reduced to its lower value (through time interval 0.5 to 0.7). Through this interval the main grid is used to compensate the required power for EV-battery charging.

In figure 12-f, the modulation-index variation of the 3-level interconnected inverter is illustrated to show how the inverter tries to change the output voltage according to the irradiance variation. Dependently, the 3-level voltage output of the inverter and main grid are shown in figure 13. The peak value of the line voltage is approximately 540V ($380\sqrt{2}$). The high-frequency output voltage of the resonant converter is given in figure 14. The output frequency is 30KHz.

So, both figures (15,16) describe the high-frequency input voltage and current of the ACT-primary winding respectively. On the other hand, the voltage and currents of the secondary winding of ACT are illustrated in both figures 17 and 18 respectively.

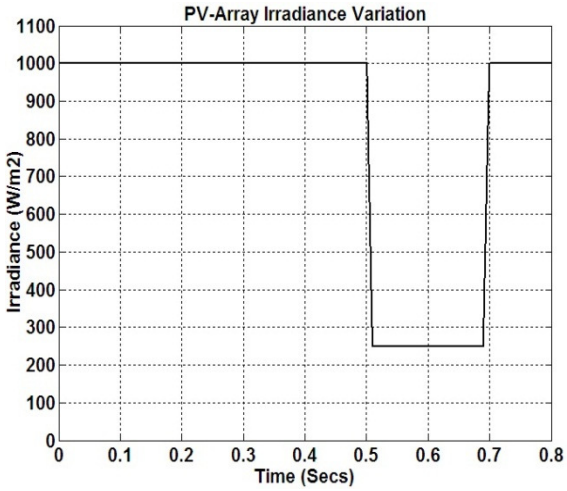

Figure 12 (a) PV-irradiance

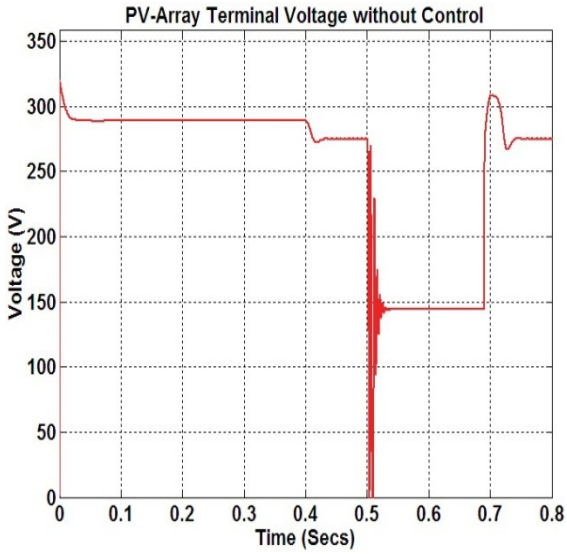

Figure 12 (b) PV-output voltage without control

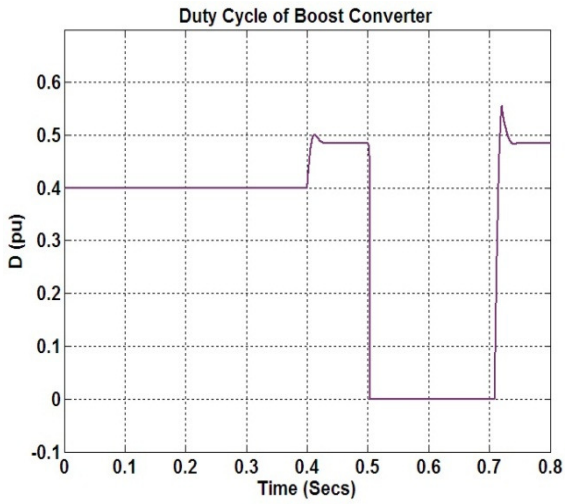

Figure 12 (c) Duty-cycle of controlled converter

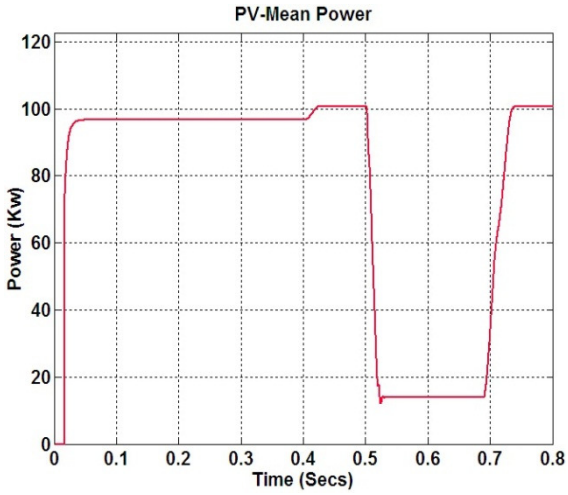

Figure 12 (d) PV-mean power

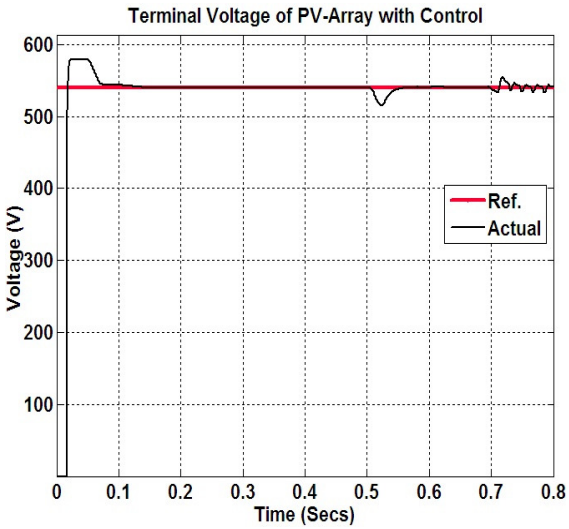

Figure 12 (e) PV-output voltage with control

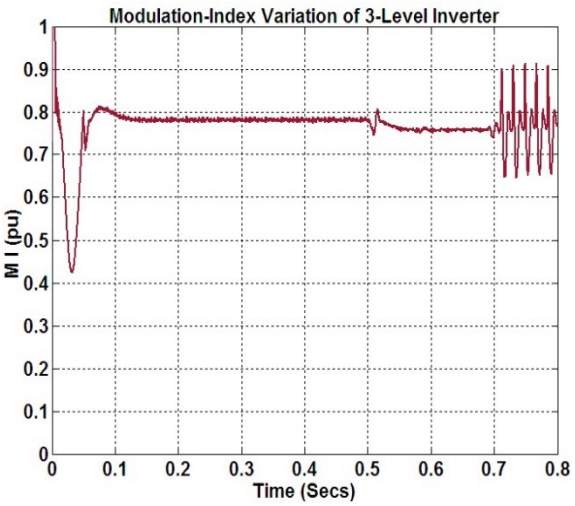

Figure 12 (f) Modulation index of inverter

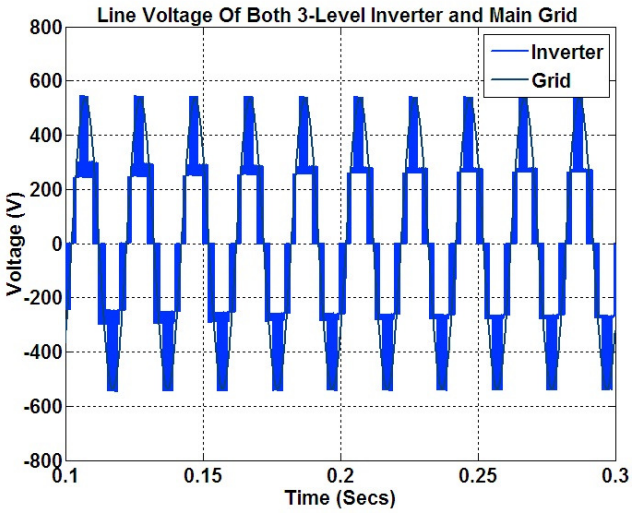

Figure 13. 3-level inverter output voltage

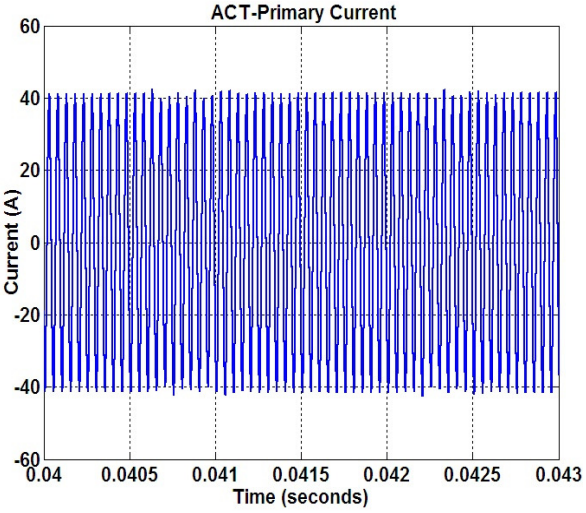

Figure. 16 ACT-primary current

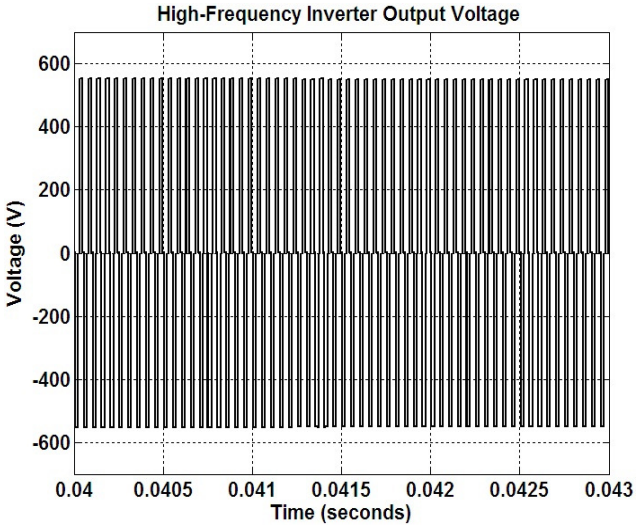

Figure 14. High frequency converter output

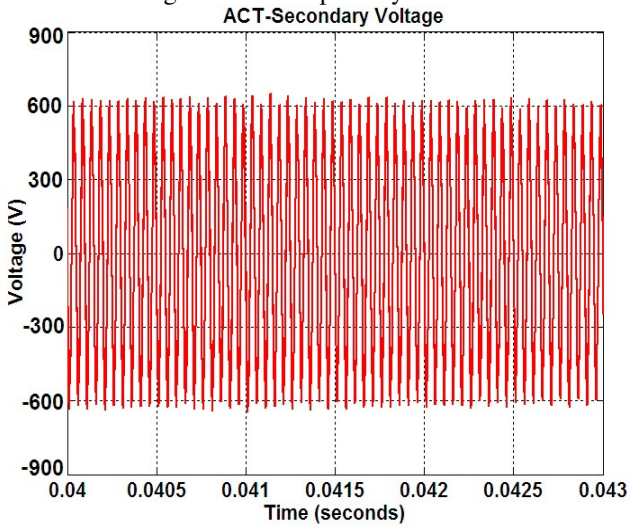

Figure 17. ACT-secondary voltage

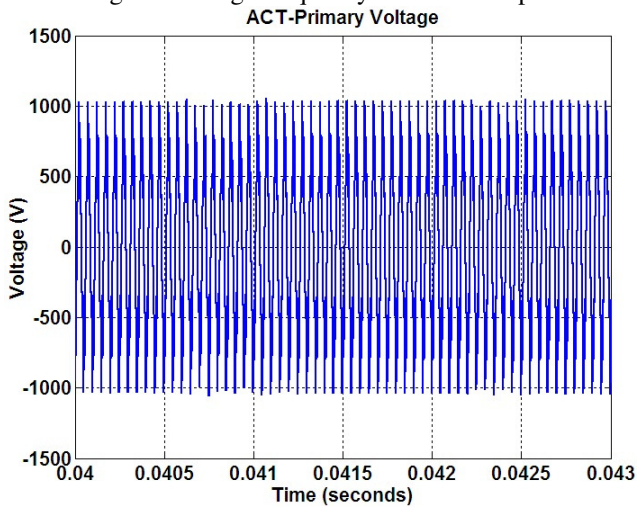

Figure 15. ACT-primary voltage

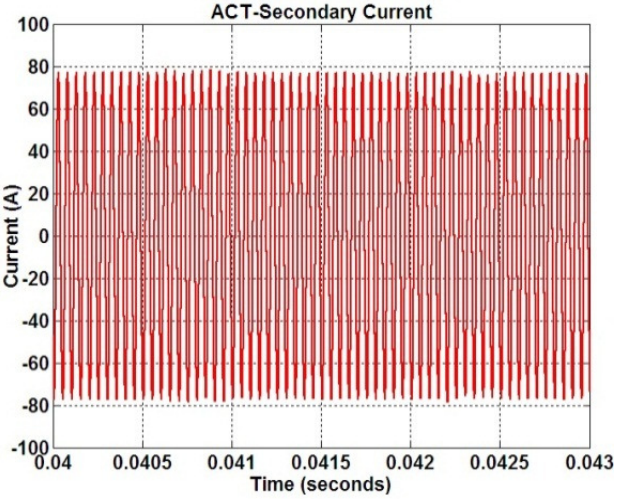

Figure. 18 ACT-primary current

The high-frequency converter is used to raise the primary voltage to approximately 1000V (peak value) and dependently the secondary-winding output voltage is approximately (600V) where turns ratio of the ACT equal (10:6). Simulation results are obtained assuming that the initial battery state of charge (SOC) equals (30%) as shown in figure 19.
Figure 20 illustrates the charging current of one EV-Honda battery through time. The current waveform is varied according to switching process of the buck converter used as a current controller for the battery.
Also, figure 21 demonstrates the battery charging voltage-level. The value of the battery-voltage is controlled to be kept constant where the charging process is achieved at constant voltage.
However, the overall average charging efficiency can be calculated as:

$$\eta_{ol} = \left(\frac{P_o}{P_i} \times 100\right) = \left(\frac{n v_b i_b}{P_m} \times 100\right)$$
$$= \left(\frac{4 \times 200 \times 90}{94000}\right) \cong 76.6\%$$

Where, v_b and $i_b$are the battery-charging voltage and current (V,A) respectively, n=number of charging batteries, P_m= PV mean power (W).
This efficiency is calculated with some approximation and with some considerations such as considering ideal switches and mathematical models for all components instead of real models. So, this study is a guide for researchers to model and simulate a public battery-charging station fed from PV-array. Also, in this research, the economic study is not considered here due to price variation from one country to another without price constancy.

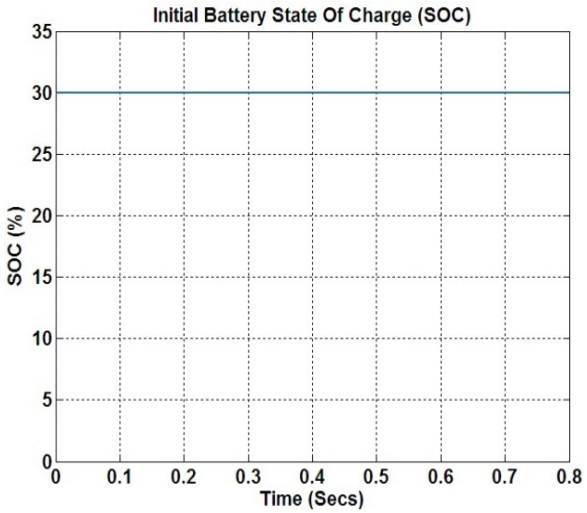

Figure19. State of charge (SOC %)

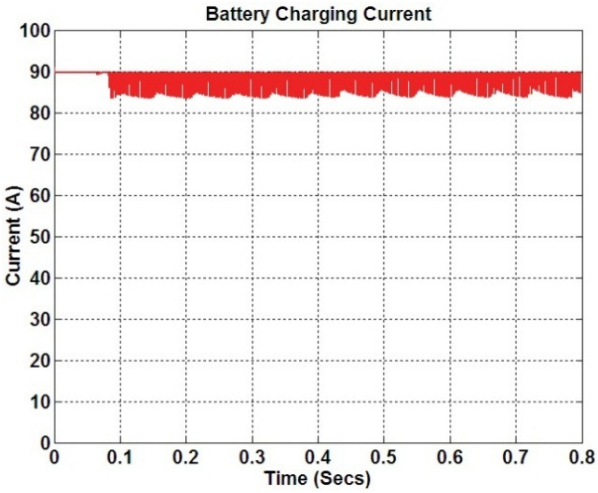

Figure 20. Charging current of battery

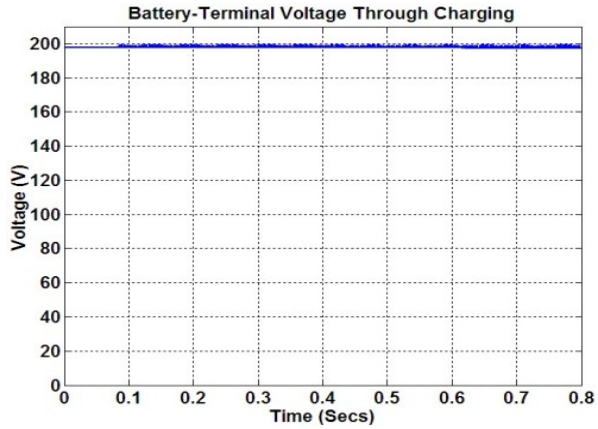

Figure 21 battery-terminal voltage through charging

6. Conclusion, Recommendation and Future Work

The paper introduces a public off-board battery-charging station fed from on-grid (OG) photovoltaic (PV) array. The proposed 100Kw-contactless charging station is modeled, designed and simulated. It comprises two main sections: station-side (stationary) section and EV (moving) section. The first section includes PV panels, maximum power point tracking (MPPT)-converter, on-grid 3-level interface inverter, and high-frequency compensated resonant converter. The second one consists of the rectifier, switched mode power converter, and battery-charging controller. An inductive-coupled power (ICP) is transferred from the station to the batteries through an air-core transformer (ACT) with large air-gap. The research introduces an m-file as a software package helping in designing ACT with its misalignment.

Smart and intelligent controllers are proposed for MPPT, interface on-grid inverter and battery-

charging converter. Also, a Matlab/Simulink software package is built and the station is tested by charging four EV-Honda batteries in the same time. Simulation results show that the overall system efficiency is improved (i.e. 76%). But, this study is technical study only not economical study. Due to rapid changing and developing in PV fabrication, inverter-converter sets, and control systems, the price of the PV-panel is decreased and changed from day to day and from place to another. So, the economic study to compute the total cost of the station will be not accurate. However, the future work will take into consideration the economic study for the proposed station.

References

1. Chwei-Sen Wang, Oskar H. Stielau, and Grant A. Covic*: Design Considerations for a Contactless Electric Vehicle Battery Charger*, In: IEEE Transaction on Industrial Electronics, VOL. 52, NO. 5, Oct. 2005, pp. 1308-1314.
2. Jesús Sallán, Juan L. Villa, Andrés Llombart, and José Fco. Sanz: *Optimal Design of ICPT Systems Applied to Electric Vehicle Battery Charge",* In: IEEE Transaction on Industrial Electronics*,* VOL. 56, NO. 6, JUNE 2009, pp. 2140-2149.
3. Juan Luis Villa, Jesús Sallán, Andrés Llombart, and José Fco Sanz: *Design of a high frequency Inductively Coupled Power Transfer system for electric vehicle battery charge*, In: Elsevier Journal of Applied Energy, Vol. 86, 2009, pp. 355-363.
4. Mansour Tabari, and Amirnaser Yazdani: *Stability of a dc Distribution System for Power System Integration of Plug-In Hybrid Electric Vehicles*, In: IEEE Transaction on Smart Grid, Vol.5, No. 5, 2014, pp. 2464-2674.
5. Seonghye Kim, and Feel-Soon Kang,: *Multifunctional Onboard Battery Charger for Plug-in electric Vehicles*, In: IEEE Transaction on Industrial Electronics, VOL. 62, NO. 6, JUNE 2015, pp. 3460-3472.
6. S. Janghorban, C. Teixeira, D. G. Holmes, P. McGoldrick, and X. Yu: *Magnetics Design for a 2.5-kW Battery Charger*, In: Australasian Universities Power Engineering Conference, AUPEC 2014, Curtin University, Perth, Australia, 28 Sep. – 1 Oct.2014, pp. 1-6.
7. Essamudin A. Ebrahim: *A Novel Approach of Bacteria-Foraging Optimized Controller for DC Motor and Centrifugal Pump Set Fed from Photo-Voltaic Array*, In: Journal of Next Generation Information Technology (JNIT), Volume 6, Number 1, February 2015, pp. 21-31.
8. D. Miskovski, and S. S. Williamson: *Modelling and Simulation of a Photovoltaic (PV) Based Inductive Power Transfer Electric Vehicle Public Charging Station*, In: IEEE Transportation & Electrification Conference and Expo (ITEC 2013), 16-19 June 2013, pp. 1-6.
9. Pierre Giroux , Gilbert Sybille, Carlos Osorio, and Shripad Chandrachood: *Grid-Connected PV Array*, Mathwork Co., 2012.
10. Mathwork Corporation: *Matlab/ Simulink 2012b*, User's Guide, USA 2012.
11. http://www.solardesigntool.com/components/module-panel-solar/Sunpower/514/SPR-305-WHT-U/specification-data-sheet.html
12. T. Esram and P. L. Chapman: *Comparison of Photovoltaic Array Maximum Power Point Tracking Techniques*, In: IEEE Transaction on Energy Conversion, Vol. 22, No. 2, June 2007, pp. 439-449.
13. Powerex Company Catalogue: *Application notes to three-level inverter technology*, First Release, June 2009.
14. Olivier Tremblay1 and Louis-A. Dessaint: *Experimental Validation of a Battery Dynamic Model for EV Applications*, World Electric Vehicle Journal Vol. 3, 2009.
15. T.Halder: *Charge Controller of Solar Photo-Voltaic Panel Fed (SPV) Battery*", In: India Inter. Conf. on Power Electronics (IICPE), 28-30 Jan, 2011, New Delhi, India, pp. 1-4.
16. D. M. Robalino et al.: *Design of a Docking Station for Solar Charged Electric and Fuel Cell Vehicles*, In: 2009 International Conference on Clean Electrical Power, 9-11 June 2009, Capri, pp. 655-660.
17. N. Harrabi, M. Soussi and A. Aitouche: *Maximum Power Control for Photovoltaic Power based on Fuzzy Takagi-Sugeno Model,* In: JEE Vol. 15, 2015, Edition 2.
18. A. El Shahat, R. Haddad and Y. Kalaani*: Lead Acid Battery Modeling for Photo-voltaic Applications*, In: JEE Vol. 15, 2015, Edition 2.